Asymmetric Twins in Boron Very Rich Boron Carbide

Journal:	*Physical Chemistry Chemical Physics*
Manuscript ID	CP-ART-03-2018-001429.R1
Article Type:	Paper
Date Submitted by the Author:	01-Apr-2018
Complete List of Authors:	Yang, Xiaokun; University of Nevada, Reno, Chemical and Materials Engineering Goddard, William; CALTECH, Beckman Institute, Center for Materials and Molecular Simulation An, Qi; University of Nevada, Reno, Chemical and Materials Engineering

Asymmetric Twins in Boron Very Rich Boron Carbide

Xiaokun Yang,[1] William A. Goddard III,[2] and Qi An[1,3*]

[1]Department of Chemical and Materials Engineering, University of Nevada, Reno,
Reno, Nevada, 89577, United States

[2]Materials and Process Simulation Center, California Institute of Technology, Pasadena,
California 91125, United States

[3]Nevada Institute for Sustainability, University of Nevada, Reno, Reno, Nevada 89557, USA

*Corresponding author E-mail: qia@unr.edu

Abstract: Twin boundaries (TBs) play an essential role in enhancing the mechanical, electronic and transport properties of polycrystalline materials. However, the mechanisms are not well understood. In particular, we considered that they may play an important role in boron very rich boron carbide ($B_{vr}BC$), which exhibits such promising properties as low density, super hardness, high abrasion resistance, and excellent neutron absorption. Here, we apply first-principles-based simulations to identify the atomic structures of TBs in $B_{vr}BC$ and their roles for the inelastic response to applied stresses. In addition to symmetric TBs in $B_{vr}BC$, we identified a new type of asymmetric twin that constitutes the phase boundaries between boron rich boron carbide ($B_{13}C_2$) and $B_{vr}BC$ ($B_{14}C$). The predicted mechanical response of these asymmetric twins indicates a significant reduction of the ideal shear strength compared to single crystals $B_{13}C_2$ and $B_{14}C$, suggesting that the asymmetric twins facilitate the disintegration of icosahedral clusters under applied stress, which in turn leads to amorphous band formation and brittle failure. These results provide a mechanistic basis towards understating the roles of TBs in $B_{vr}BC$ and related superhard ceramics.

Keywords: Twin boundary, DFT, Boron carbide, Hardness, Biaxial strain, Mechanical property

1. Introduction

Twin boundaries (TBs), separating two crystals through a mirror plane, form during the processes of crystal growth, annealing and deformation[1,2] and are ubiquitous in many crystalline solids. In contrast to traditional grain boundaries (GBs), which are incoherent, TBs are generally exhibit small lattice mismatch so that they are energetically more stable. Consequently, TBs significantly affect the mechanical, electronic and transport properties of realistic materials[3–5]. In particular, the formation of nanoscale twins can significantly affect the plasticity and strength of metals and ceramics. For example, nanotwinned Cu is ten times *stronger* than coarse-grained Cu.[4] Another example is that *nanotwins* in ceramics have been found to *dramatically enhance the strength and hardness of diamond and boron nitride*[6,7].

TBs can be identified easily in relatively simple systems such as FCC, BCC, and HCP metals. However, they become quite complex for more complicated crystal structures that exhibit secondary and tertiary structural hierarchy. For example, Fujita *et al.*[8] used high-resolution transmission electron microscopy (HRTEM) to discover a new type of TB in carbon rich boron carbide (B_4C) where the angle between the (100) and (010) rhombohedral planes differs by ~2° on either side of the TBs. This type of TBs is referred to as an "asymmetric twin" because of the loss of twin symmetry. Our further study combining HRTEM and first-principles-based simulations indicated that this "asymmetric twin" in B_4C is associated with the distribution of carbon atoms into various positions within the 12-atom icosahedron[9].

Boron carbides have been widely used as high performance ceramic materials where hardness and weight are critical because of such promising properties as low density, ultra-high hardness, good thermal stability, and low material costs[10–14]. It is also of great interest for nuclear applications because of its high neutron absorption and self-healing capacities[15]. Similar to other ceramics and metal alloys, the mechanical properties of boron carbides depend strongly on chemical composition, microstructure, and fabrication processes[14,16–20]. Boron carbides, consisting of a 12-atom icosahedron with a 3-atom chain in a rhombohedral unit, possess very complex crystalline structures. They have a wide composition range from 8.8 to 20 at.% C[14,16,20,21]. Beyond ~20 at.% C, a mixture of B_4C and graphite is often observed. Below ~8 at.% C α-boron usually co-exists with B_4C[20,22]. Only two stoichiometries have been proposed as candidates for the stable boron carbide:

(1) the B_4C with the configuration $(B_{11}C_p)CBC$ where the icosahedral carbon is located at a polar site that connects directly to other icosahedra[13];

(2) the boron rich boron carbide ($B_{13}C_2$) with the atomic configuration $(B_{12})CBC$[23].

The atomic structures in the regime below ~13.3 at.% C (or $B_{vr}BC$) have not previously been identified, but it was proposed that they may be the combination of B_{12}, $B_{11}C$, $B_{10}C_2$, and B_9C_3 icosahedra and CCC, CBC, CCB, CBB, BCB, and BBB chains.

Previous studies [24] have shown that high density twins can be introduced experimentally into B_4C, $B_{13}C_2$ and $B_{vr}BC$[16]. Close examinations of these materials showed that both symmetric twins and "asymmetric twins" are present in highly twinned samples of B_4C and $B_{vr}BC$[8,16]. Previous study suggests that asymmetric twins in B_4C form because the C atoms can be distributed in polar sites (connected to icosahedra) or equatorial sites (connected to CBC chain) within the $(B_{11}C)$ icosahedron[9]. As B content increases to $B_{13}C_2$, only symmetric twins can be observed because the icosahedral carbon is replaced by B atoms to form (B_{12}) icosahedron[9,23]. Recently, Cheng *et al.* observed two types of growth twins in the $B_{vr}BC$ samples ($B_{7.8}C$ and $B_{10.2}C$) using HRTEM. One type of twin is the conventional symmetric twin with a twin angle of about 72.8 ± 0.2°[16]. This type of twin agrees well with our QM predicted twins in $B_{13}C_2$ in which (B_{12})CBC configurations are on both sides of TBs[9]. However, most twins in the $B_{vr}BC$ samples are "asymmetric twins" with twin angles of 72.8 ± 0.2° and 74.1 ± 0.2° on two sides of TBs[16]. It was speculated that the increased population of asymmetric twins could be associated with the monoclinic distortion of the structure caused by the excess boron[16]. However, the atomic structures and formation mechanisms have not been explained. Previous study only examined the crystal structures for $B_{14}C$ but provides no information on the possible twinned structures in $B_{vr}BC$[25]. Clearly the formation of "asymmetric twins" must be related directly to the hierarchical levels of $B_{vr}BC$ structures. We recently investigated the deformation mechanisms of symmetric twins in $B_{13}C_2$ and found that these nanotwins significantly decrease the strength of single crystal $B_{13}C_2$.[23] This is in contrast with the nanotwins in B_4C where the nanotwins increase the strength of the single crystal B_4C[24]. However, it remains unclear how the nanotwins affects the mechanical properties of $B_{vr}BC$.

In the present study, we first apply first-principles-based simulations (density functional theory (DFT) at the Perdew−Burke−Ernzerhof (PBE) level) to demonstrate that **the "asymmetric twins" in $B_{vr}BC$ are actually the phase boundaries of (B_{12})CBC and (B_{12})CBB.** Particularly, in the (B_{12})CBB phase, the C-B-B chain can be either a kinked chain or a linear chain, as discussed in our previous study[25]. Then we examined the response of these asymmetric twins to applied stress and derived the stress−strain relationships, the ideal shear strength, and the failure mechanisms. We find that the asymmetric twins lead to a lower ideal shear strength than those of both (B_{12})CBC and (B_{12})CBB, suggesting a softening effect. However, under the stress conditions appropriate for an indentation experiment, we find that **the asymmetric twins lead to a higher critical stress than that of (B_{12})CBB, but lower than that of (B_{12})CBC**. The failure mechanism for asymmetric twins arises from the interaction between the icosahedral clusters and the C-B-B chains under pure shear deformation. While under indentation the failure initiates from the interactions of both C-B-B and C-B-C chains with their nearest icosahedra.

2. Computational methodology

All the DFT calculations were performed with the VASP package[26–28], using the PBE functional and the projector augmented wave (PAW) method to account for the core−valence interactions[29]. The electron partial occupancies were determined using the tetrahedron method with Blöchl corrections. The energy cutoff for the plane wave expansion was 600 eV and Brillouin zone integration was performed on Γ-centered symmetry-reduced Monkhorst−Pack meshes with a fine resolution of $2\pi \times 1/40$ Å^{-1} for all calculations except for the shear deformation. The energy error for terminating electronic self-consistent field (SCF) and the force criterion for the geometry optimization were set equal to 10^{-6} eV and 10^{-3} eV/Å, respectively.

To determine the ideal shear strength for the asymmetric twinned structure, we applied the pure shear deformation along the TBs by imposing the shear strain along the twin plane while allowing full structural relaxation for the other five strain components[30]. To simulate the mechanical response under indentation experiments, we applied biaxial shear deformation on the asymmetric twined structure. This simulation aims at mimicking deformation under the indenter by imposing the relations $\sigma_{zz} = \sigma_{zx} \times \tan \Phi$ where σ_{zz} is the normal stress, σ_{zx} is the shear stress and Φ is the centerline-to face angle of the indenter ($\Phi = 68°$ for Vickers indenter)[7]. The other four strain components are relaxed in biaxial shear deformations. The residual stresses after relaxing were less than 0.5 GPa for both pure shear and biaxial shear deformation. A more approximate $2 \times 2 \times 2$ k-point grid mesh in the Brillouin zone was applied in both pure shear and biaxial shear deformation. Since the shear strain is constrained in the deformation, the stress of the system may become negative after the structure changes or fails.

3. Results and discussion

To characterize the asymmetric twins in $B_{vr}BC$, two boron carbide configurations were considered: $(B_{12})CBC$ and $(B_{12})CBB$. Fig. 1(a) displays the $(B_{12})CBC$ crystal structure (2 × 1 × 4 supercell) with $R\bar{3}m$ space group where the B_{12} icosahedral cluster is located on the corner and the C-B-C chain is along the [111] rhombohedral directions. Here, crystal planes and directions are given using 3-index rhombohedral notation. The angle between (100) and (010) was measured to be $\alpha = 73.24°$ in the $(B_{12})CBC$ crystal, as shown in Fig. 1(a).

For $(B_{12})CBB$ crystal, two atomic structures were considered: bent C-B-B chain $(B_{12})bCBB$, and linear C-B-B chain $(B_{12})lCBB$. Our previous study indicated that the $(B_{12})bCBB$ is more stable than the $(B_{12})lCBB$ by 0.3 eV/unit-cell because it has one 3c-2e bond and two 2c-2e bonds instead of three 3c-2e bonds per unit cell, making $(B_{12})bCBB$ more favorable [25]. The crystalline structure (2 × 1 × 4 supercell) for $(B_{12})bCBB$ is displayed in Fig. 1(b) with the measured angle $\alpha' = 71.80°$. In contrast, the crystalline structure (2 × 1 × 4 supercell) for $(B_{12})lCBB$ is displayed in Fig. 1(d) with the measured angle $\alpha' = 73.70°$.

To determine the atomic structures of asymmetric twins, we constructed twinned models with the {100} plane as the TB; here two layers of $(B_{12})CBC$ are on one side and two layers of either $(B_{12})bCBB$ or $(B_{12})lCBB$ structures are on the other side. We named the 1st nearest layer to the middle TB on the $(B_{12})CBB$ side the layer I of $(B_{12})CBB$, and named the other layer the layer II of $(B_{12})CBB$ (Fig. 1(c),(e)). Similarly, on the $(B_{12})CBC$ side, the 1st nearest layer to the middle TB is the layer I of $(B_{12})CBC$, and the other layer is the layer II of $(B_{12})CBC$ (Fig. 1(c),(e)).

The twinned model with (B_{12})*b*CBB and (B_{12})CBC contains 120 atoms and was relaxed by DFT simulations, leading to the cell parameters of a = 10.339 Å, b = 5.170 Å, c = 18.087 Å, α = 90.8°, β = 89.2°, and γ = 113.4° with a density of 2.456 g/cm^3. The C-B-B chains in layer II become almost linear with a C-B-B angle of 176.7^o while the C-B-B chains in layer I remain bent with a C-B-B angle of 94.3^o, as shown in Fig. 1(c). Therefore, the middle TB connects (B_{12})CBC and (B_{12})*b*CBB while the other edge TB connects (B_{12})CBC and (B_{12})*l*CBB. This is because the lattice mismatch between (B_{12})CBC and (B_{12})*b*CBB is larger than lattice mismatch between (B_{12})CBC and (B_{12})*l*CBB. This turns one layer of (B_{12})*b*CBB to (B_{12})*l*CBB in this twinned model. The inclination angles were measured to be α = 72.90° and α' = 74.35°, as shown in Fig. 1(c), which agree very well with experimental measurements of α = 72.8 ± 0.2° and α' =74.1 ± 0.2°[16].

Our results suggest that the asymmetric twins observed experimentally[16] are actually the phase boundary of two phases (B_{12})CBC and (B_{12})CBB. Therefore, the new asymmetric twins are associated with the distribution of boron atoms into various positions within 3-atom chain and chain deformation (bent vs linear), which is different from the asymmetric twins in B_4C[9] where they are associated with the distribution of carbon atoms into the icosahedron. Our QM simulations predict the interfacial energy of asymmetric twins in $B_{vr}BC$ to be 108.4 mJ/m^2, which is higher than that of asymmetric twins in B_4C (83.2 mJ/m^2)[9] and much higher than that of symmetric twins in $B_{13}C_2$ (40.6 mJ/m^2)[23]. This higher interfacial energy can be ascribed to the lattice mismatch caused by the kinked C-B-B chain.

In order to examine how the linear C-B-B chain affects the twinned structures, a twinned model with (B_{12})*l*CBB (Fig.1(e)) was constructed and relaxed by DFT simulations, leading to the cell parameters of a = 10.335 Å, b = 5.167 Å, c = 18.130 Å, α = 90.6°, β = 90.6°, and γ = 113.7°

with a density of 2.456 g/cm^3. The inclination angles were measured to be α = 73.27° and α' = 74.05°. The angle difference is ~0.8°, which is slightly lower than the experimental measurements of 1.3°[16]. The interfacial energy for this twinned model is predicted to be 7.0 mJ/m^2 if the referent structures are (B_{12})CBC and (B_{12})*l*CBB. Although the small lattice mismatch between (B_{12})CBC and (B_{12})*l*CBB leads to much lower interfacial energy, this model is 0.1 eV/unit-cell higher in energy than the above twinned model mixing (B_{12})*b*CBB and (B_{12})CBC, suggesting that the above model is the most plausible asymmetric twins under experimental conditions. Therefore, we will focus on the (B_{12})CBC−(B_{12})*b*CBB twinned model when examining the mechanical properties. We will also examine the (B_{12})CBC−(B_{12})*l*CBB twinned model for comparison.

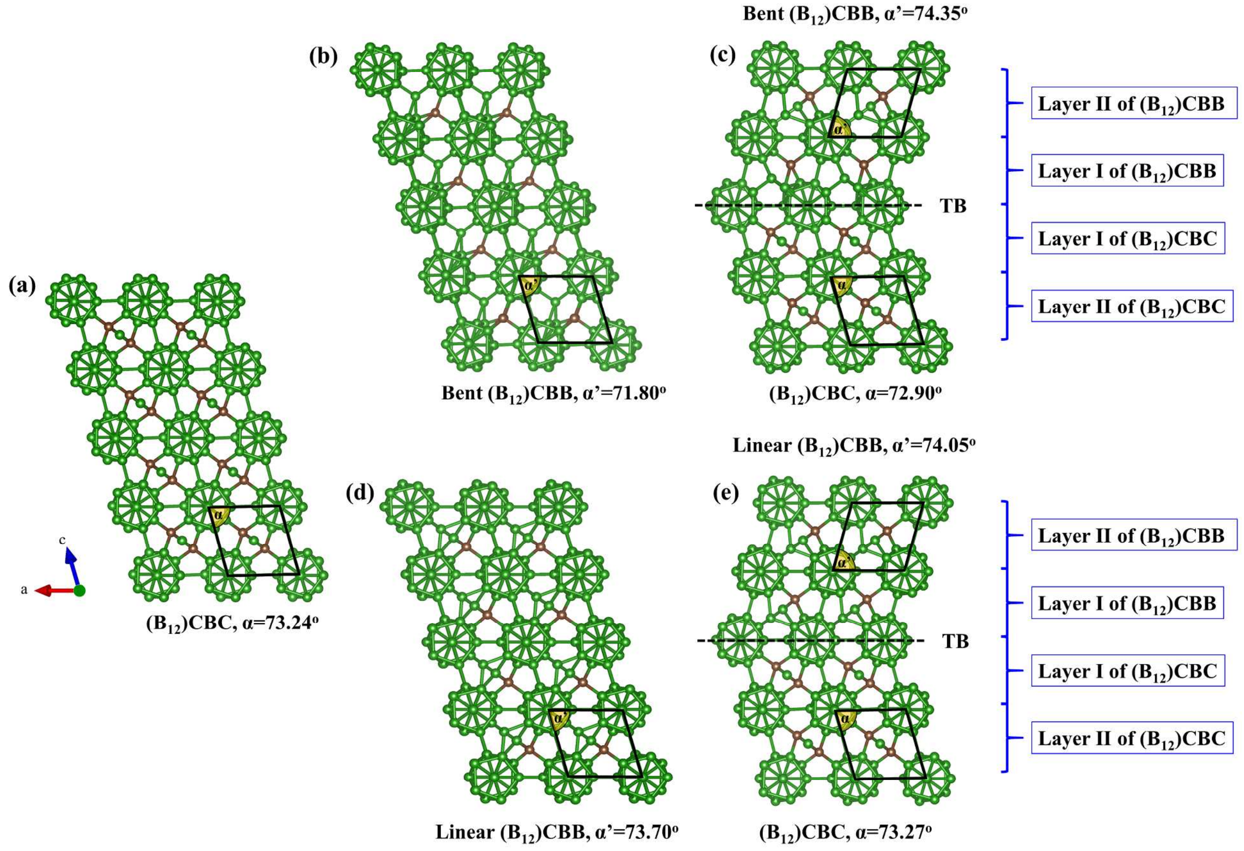

Fig.1 The atomic models from the DFT simulations: (a) single crystal (B_{12})CBC , (b) single crystal (B_{12})*b*CBB, (c) (B_{12})CBC−(B_{12})*b*CBB asymmetric twin, (d) single crystal (B_{12})*l*CBB, and (e)

(B_{12})CBC−(B_{12})*l*CBB asymmetric twin. The TB plane is represented by a dashed black line. The boron and carbon atoms are represented by green and sienna balls, respectively.

In order to understand the mechanical response of asymmetric twins we applied pure shear deformation on the twinned (B_{12})CBC−(B_{12})*b*CBB model and compared with the single crystal (B_{12})CBC and (B_{12})*b*CBB. Previous experimental studies [11] and our previous QM calculations [31] suggest that the most plausible slip system for B_4C is the (001)[100]. Considering the structure similarity, we sheared the single crystal (B_{12})CBC and (B_{12})*b*CBB along the (001)[100] slip system and sheared the twinned model along the TBs, which corresponds to the {001} plane. The shear-stress−shear-strain relationships for crystalline (B_{12})CBC, (B_{12})*b*CBB and twinned (B_{12})CBC−(B_{12})*b*CBB structures are displayed in Fig. 2(a). The ideal shear strength for the asymmetric twinned model is 22.1 GPa, which is 23.7 GPa and 7.9 GPa lower than those for the single crystal (B_{12})CBC (45.8 GPa) and (B_{12})*b*CBB (30.0 GPa), respectively. Thus, the presence of the nanoscale twins significantly reduces the ideal shear strength of the single crystal (B_{12})CBC and (B_{12})*b*CBB. This suggests that the mechanical failure likely initiates at the asymmetric TB regions in B_{vr}BC.

In order to understand how the linear C-B-B chain affects the failure of the asymmetric twinned model, we applied pure shear deformation on twinned (B_{12})CBC−(B_{12})*l*CBB model and compare to the (B_{12})CBC and (B_{12})*l*CBB. The shear-stress−shear-strain relationships for single crystal (B_{12})CBC, (B_{12})*l*CBB and twinned (B_{12})CBC−(B_{12})*l*CBB model are displayed in Fig. 2(b). The ideal shear strength for twinned (B_{12})CBC−(B_{12})*l*CBB model is 23.0 GPa, which is much lower than those for single crystal (B_{12})CBC (45.8 GPa) and (B_{12})*l*CBB (30.0 GPa). It is slightly higher than twinned (B_{12})CBC−(B_{12})*b*CBB model although the twinned (B_{12})CBC−(B_{12})*b*CBB model is slightly lower in energy. The failure mechanism of these two structures will be compared and discussed in the following paragraphs.

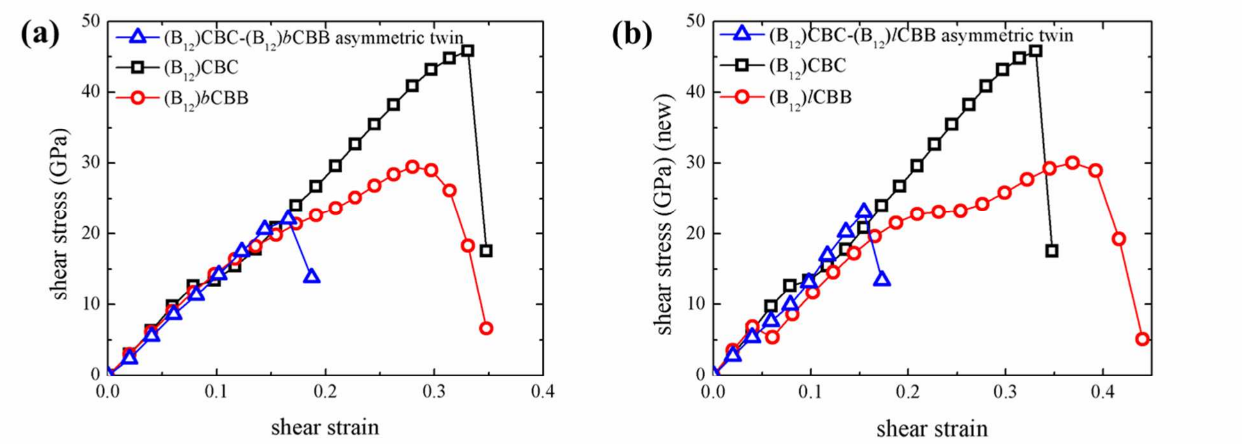

Fig. 2 Shear-stress−shear-strain relationship under pure-shear deformation of (a) the $(B_{12})CBC-(B_{12})bCBB$ asymmetric twin (blue Δ), the single crystal $(B_{12})CBC$ (black □), and the single crystal $(B_{12})bCBB$ (red ○) and (b) the $(B_{12})CBC-(B_{12})lCBB$ asymmetric twin (blue Δ), the single crystal $(B_{12})CBC$ (black □), and the single crystal $(B_{12})lCBB$ (red ○).

Our previous studies concluded that brittle fracture in B_4C arises from the shear-induced cracking of the $(B_{11}C)$, which subsequently leads to amorphous band region, which then induces cavitation and eventually crack opening[31,32]. To understand how the “asymmetric twins” affect the brittle failure process in $B_{vr}BC$, we examined the detailed structural changes under pure shear deformation.

In the $(B_{12})CBC-(B_{12})bCBB$ asymmetric twin, the structure experiences elastic deformation as the shear strain increases from 0 to 0.166. In the two layers of the “asymmetric twins” model, only C-B-B chains in layer I are bent while the C-B-B chains in layer II remaining approximately linear. As the shear strain increases to 0.166, the linear chains in layer II (C6-B43-B107) are deformed from 176.7° to 107.0°, as shown in Fig. 3(b). Meanwhile, the B1−B13 bond within the icosahedron is stretched from 1.820 Å to 1.899 Å. As the shear strain increases further to 0.187 (Fig. 3(c)), the B1−B13 bond breaks with the bond distance increasing to 2.703 Å. Meanwhile, the C6 in C-B-B chain is bonded to B1 within the icosahedron (bond distance is 1.803 Å). This leads to the deconstruction of the icosahedra, releasing the shear stress from 22.1 GPa to 13.8

GPa. The failure arises from the interaction between the (B_{12}) icosahedra and the C-B-B chains in layer II while the chains in layer I remain intact. During the whole failure process, the structure in the (B_{12})CBC region does not disintegrate. This is consistent with our prediction that the ideal shear strength of (B_{12})CBC is much higher than that of (B_{12})CBB.

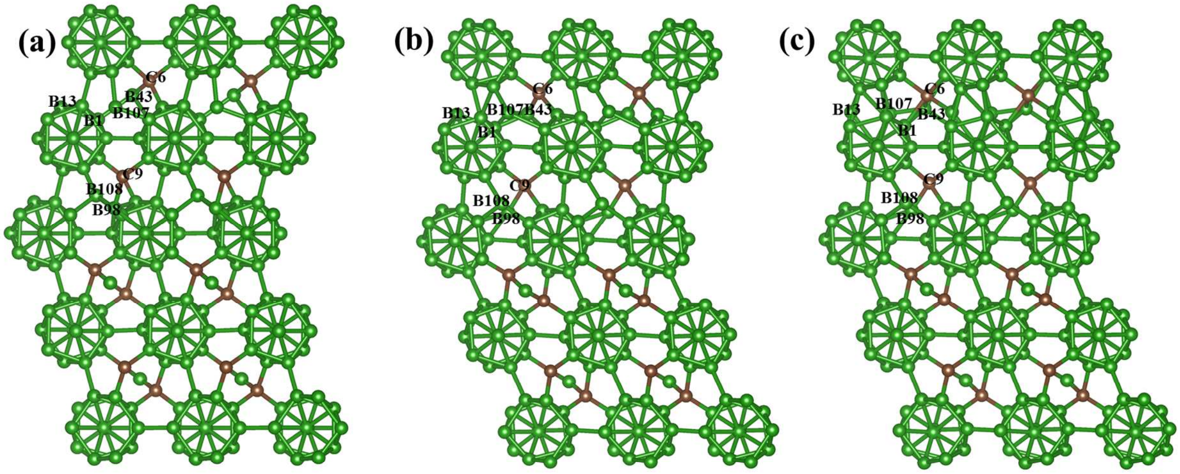

Strain = 0 **Strain = 0.166** **Strain = 0.187**

Fig. 3 Structure evolution of (B_{12})CBC−(B_{12})*b*CBB asymmetric twin under pure shear deformation: (a) Intact structure; (b) The structure at 0.166 strain before failure, the B-B bond within the icosahedra is stretched in layer II of (B_{12})CBB. (c) The failed structure at 0.187 strain.

Detailed structural changes of (B_{12})CBC−(B_{12})*l*CBB asymmetric twin under pure shear deformation are analyzed and shown in Fig. 4. The linear C-B-B chains in both layers are bent when the shear strain is applied. The angle of C6-B43-B107 in layer II of (B_{12})CBB region bends from 176.7^{o} to 116.0^{o} at 0.155 strain, causing the middle B43 in C-B-B chain to approach the nearest icosahedron (1.883 Å). The C9-B108-B98 angle in layer I of (B_{12})CBB region also bends, as shown in Fig. 4(b), similarly to the (B_{12})CBC−(B_{12})*b*CBB twin. Meanwhile, the B1−B13 bond within icosahedron is stretched from 1.803 to 1.827 Å. As the shear strain further increases to 0.173 (Fig. 4(c)), the B1−B13 bond breaks with a bond distance increasing to 2.755 Å, and the chain atom C6 is bonded to the cage atom B1 with a bond distance of 1.805 Å. This leads to the deconstruction of icosahedra, releasing the shear stress from 23.0 GPa to 13.4 GPa. In layer I region, B98 and B108 atoms slightly adjust their positions leading to the bended C-B-B chain angle of 101.8°. Similar to $(B_{12})CBC{-}(B_{12})bCBB$, the brittle failure of $(B_{12})CBC{-}(B_{12})lCBB$ asymmetric twin also arises from the interaction between the (B_{12}) icosahedra and the C-B-B chains in the layer II of $(B_{12})CBB$ region.

Our previous study[23] showed that the brittle failure in $(B_{12})CBC$ arises from the direct disintegration of icosahedra, which leads to higher ideal shear strength. This suggests that the $(B_{12})CBC$ is stronger than $B_{vr}BC$. Therefore, it is essential to decrease the B content to improve the strength of boron carbide. The failure process of asymmetric twinned structure is similar to crystalline $(B_{12})bCBB$[25] where the B1−B13 bond breaks, leading to the deconstruction of icosahedra.

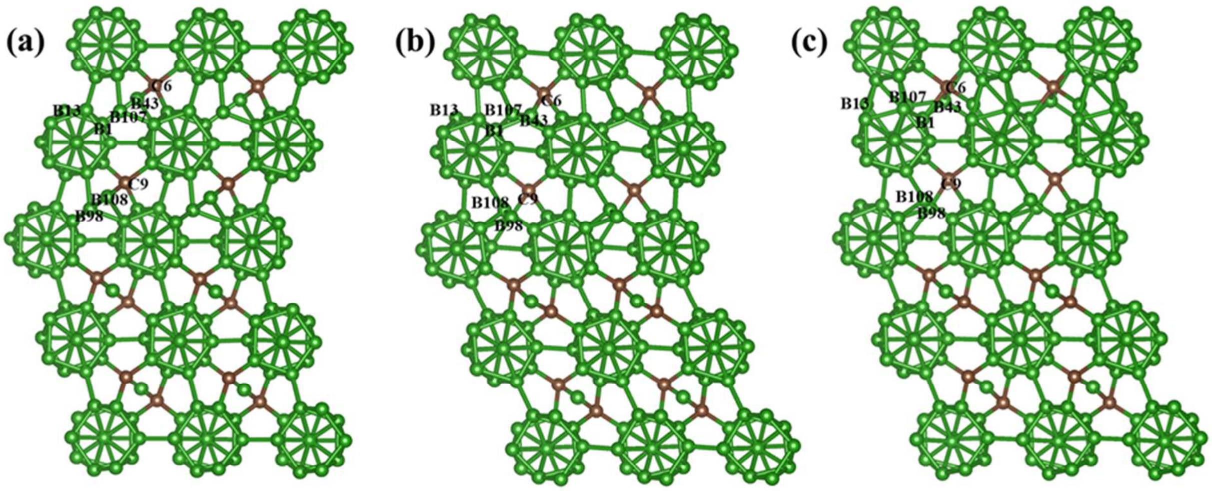

Strain = 0 **Strain = 0.155** **Strain = 0.173**

Fig. 4 Structure evolution of $(B_{12})CBC{-}(B_{12})lCBB$ asymmetric twin under pure shear deformation: (a) Intact structure; (b) The structure at 0.155 strain before failure, the B-B bond within the icosahedra is stretched in the upper half $(B_{12})CBB$ region. (c) The failed structure at 0.173 strain.

We suggest that micro- and nanoindentation experiments could be carried out to validate our predicted strength of asymmetric twinned structures, crystalline $(B_{12})CBC$ and $(B_{12})CBB$. However, the stress conditions under indentation experiments are very complex compared to our simulated pure shear deformation. To predict material behaviors under indentation experiments, we performed biaxial shear deformation to mimic the stress conditions under indentation[7]. The shear-stress−shear-strain relationships for the asymmetric twinned structures, single crystal (B$_{12}$)CBC and single crystal (B$_{12}$)CBB are shown in Fig. 5. The (B$_{12}$)CBC−(B$_{12}$)*b*CBB asymmetric twin has a maximum shear stress of 22.3 GPa, which is 22.0% lower than that of single crystal (B$_{12}$)CBC (28.6 GPa). However, it is higher than that of single crystal (B$_{12}$)*b*CBB (20.8 GPa). For the (B$_{12}$)CBC−(B$_{12}$)*l*CBB asymmetric twin, the maximum shear stress is 26.5 GPa, which is 4.2 GPa and 5.7 GPa higher than that of the (B$_{12}$)CBC−(B$_{12}$)*b*CBB asymmetric twin and single crystal (B$_{12}$)*l*CBB, respectively; but it is lower than that of single crystal (B$_{12}$)CBC. These results indicate that the hardness of the (B$_{12}$)CBC−(B$_{12}$)*l*CBB asymmetric twin should be higher than that of the single crystalline (B$_{12}$)*l*CBB but lower than that of the single crystal (B$_{12}$)CBC.

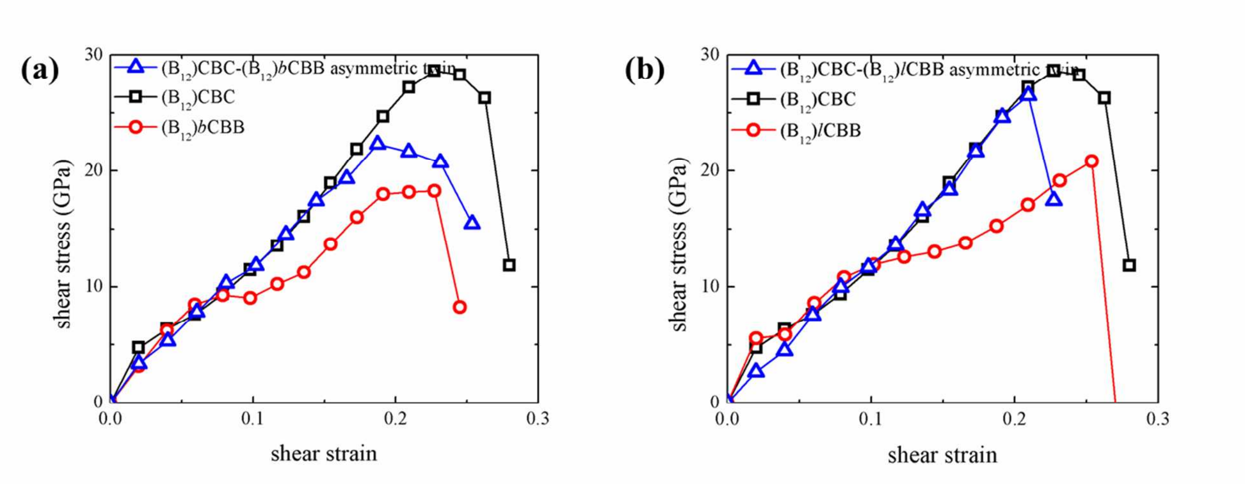

Fig. 5 Shear-stress−shear-strain relationship under biaxial shear conditions of (a) the (B$_{12}$)CBC−(B$_{12}$)*b*CBB asymmetric twin (blue Δ), the single crystal (B$_{12}$)CBC (black □), and the single crystal (B$_{12}$)*b*CBB (red ○) and (b) (B$_{12}$)CBC−(B$_{12}$)*l*CBB asymmetric twin (blue Δ), the single crystal (B$_{12}$)CBC (black □), and the single crystal (B$_{12}$)*l*CBB (red ○).

The detailed deformation processes of the $(B_{12})CBC-(B_{12})\mathit{b}CBB$ asymmetric twin under biaxial shear conditions are displayed in Fig. 6. Since a compressive stress is applied, the upper $(B_{12})CBB$ and lower $(B_{12})CBC$ regions experience different failure processes. As the shear strain increases to 0.187, the C6-B43-B107 chain in layer II of $(B_{12})CBB$ region bends to 154.4^{o} (shown in Fig. 6(b)). A slightly stress release is observed as the shear strain increases from 0.187 to 0.209. By examining the detailed structural change, we find that the C-B-B chain in layer I of $(B_{12})CBB$ region bends from 117.2^{o} to 100.0^{o} by adjusting the position of B98 and B108 atoms. As the shear strain further increase to 0.254, the adjusted chain atom B108 bonds with the B63 from icosahedra in layer I of $(B_{12})CBB$ region. Therefore, the icosahedra in layer I of the $(B_{12})CBB$ region are deconstructed (shown in Fig. 6(d)) by breaking the icosahedral B63-B68 bond. Meanwhile, the icosahedra in TB region are deformed as well because of the highly compressive stress. A new B68-B33 bond is formed, connecting two adjacent icosahedra in $(B_{12})CBB$ and TB regions. Interestingly, when the twinned structure is deconstructed, the C6-B43-B107 chain in layer II of $(B_{12})CBB$ region turns back to 172.6^{o}.

Different from pure shear conditions, under biaxial shear conditions, structure in $(B_{12})CBC$ region is deformed, but not destroyed. While the $(B_{12})CBB$ region is deconstructed. The originally linear C10-B95-C1 chain in layer I of $(B_{12})CBC$ region continuously bends when shear strain increases. The B4-B80 bonds in the layer II of $(B_{12})CBC$ region initially forms at 0.187 strain and then breaks at 0.254 strain. The icosahedra in $(B_{12})CBC$ region are not deconstructed, but the C10 atom from the bent C-B-C chain in layer I of the $(B_{12})CBC$ region bonds to B55, causing the B35-B55 icosahedral bond breaking within TB region, thus contributes to the fully deconstruction of the twinned structure.

Therefore, under biaxial shear conditions, the (B_{12})CBC−(B_{12})*b*CBB asymmetric twin fails in both layer I of the (B_{12})CBB and the TB regions because of three main factors: (1) the interaction between C-B-B chain and icosahedra in layer I of the (B_{12})CBB region; (2) the interaction between C-B-C chain and icosahedra in layer I of the (B_{12})CBC region; and (3) the highly compressive stress condition.

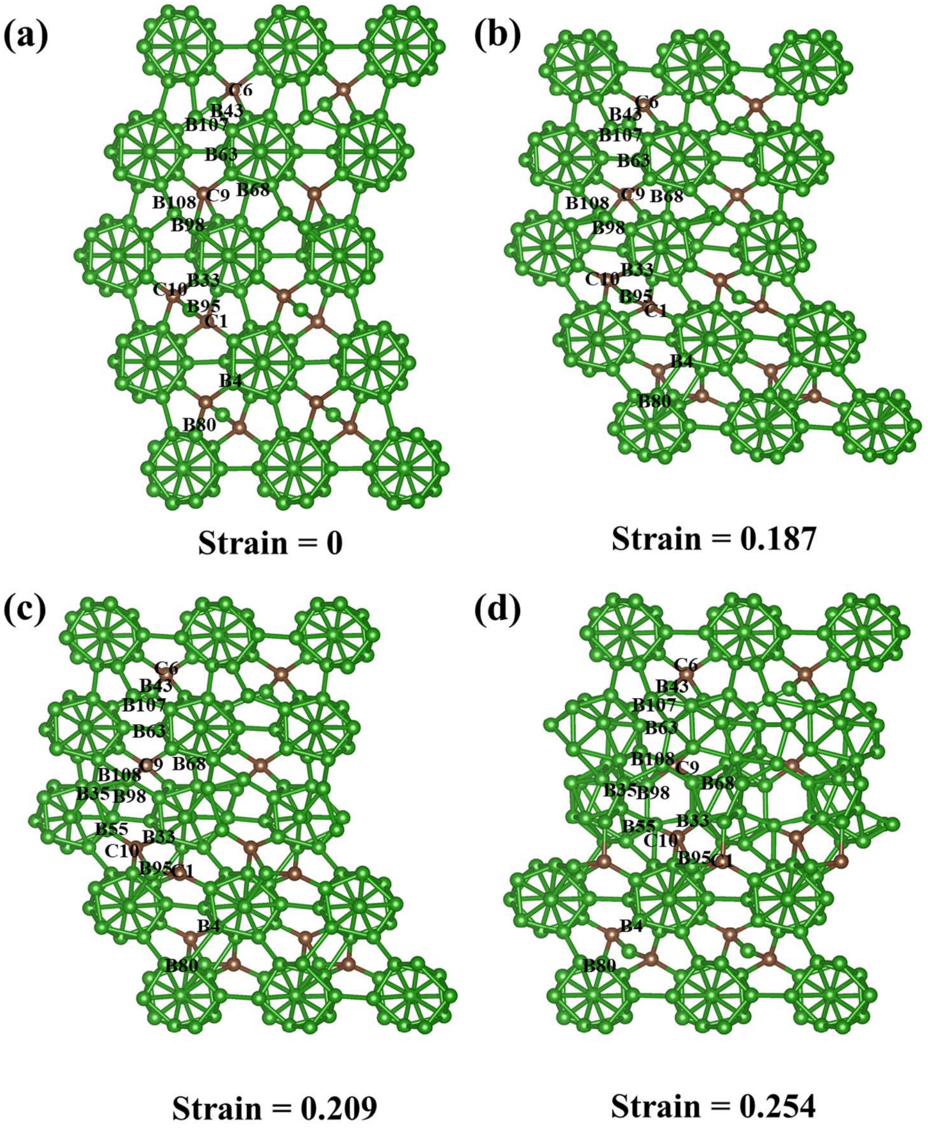

Strain = 0

Strain = 0.187

Strain = 0.209

Strain = 0.254

Fig. 6 Structure evolution of the (B_{12})CBC−(B_{12})*b*CBB twin under biaxial shear deformation: (a) Intact structure; (b) The structure at 0.187 strain before failure, both C-B-B and C-B-C chains in layer II bend; (c) The structure at 0.209 strain before failure; (d) The failed structure at 0.245 strain.

The detailed deformation processes of the $(B_{12})CBC-(B_{12})lCBB$ asymmetric twin under biaxial shear deformation are displayed in Fig. 7. As the shear strain increases to 0.209, all C-B-B and C-B-C chains bent slightly without any bond breaking as shown in Fig. 7(b). However, the icosahedra in both $(B_{12})CBB$ and $(B_{12})CBC$ regions are deformed while TB region remains intact as the shear strain further increase to 0.227 (shown in Fig. 7(c)). In $(B_{12})CBB$ region, icosahedra in both layer I and layer II are deconstructed by pressing the B51 in layer II down and forming a new B51-B107 bond with C-B-B chain. Meanwhile, the C9 from C-B-B chain in layer I forms a new bond to B68 from icosahedra of the layer I in $(B_{12})CBB$ region, causing the B68-B56 icosahedral bond break, which leads to the deconstruction of the whole $(B_{12})CBB$ region. In $(B_{12})CBC$ region, the layer II icosahedra are also deconstructed at 0.277 strain by the interaction between C8-B42-C5 chain and the icosahedra, as shown in Fig. 7(c).

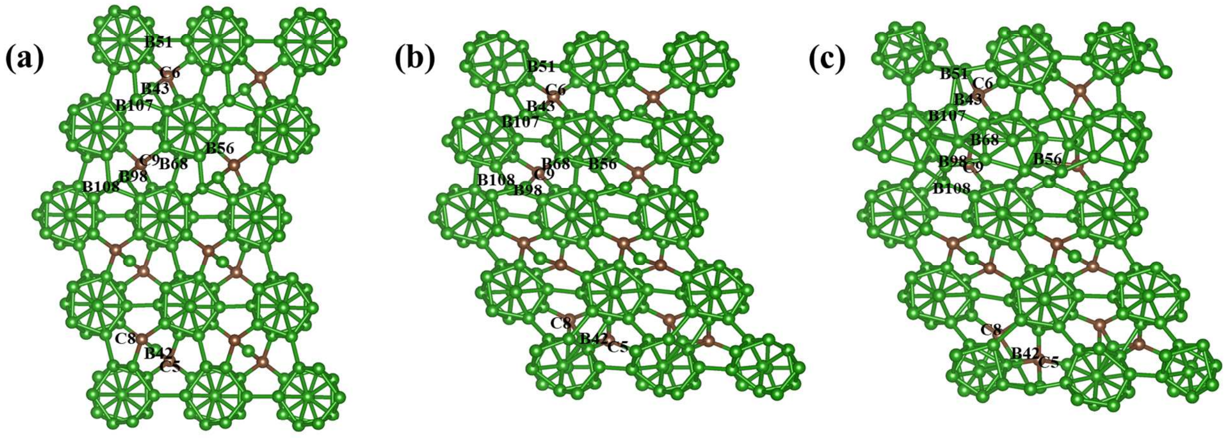

Strain = 0 **Strain = 0.209** **Strain = 0.227**

Fig. 7 Structure evolution of the $(B_{12})CBC-(B_{12})lCBB$ asymmetric twin under biaxial shear deformation: (a) Intact structure; (b) structure at 0.209 strain before failure; (c) failed structure at 0.227 strain.

4. Conclusion

In summary, we used first-principles-based simulations to identify a new type of "asymmetric twins" in $B_{vr}BC$. The new "asymmetric twins" are actually a phase boundary of two configurations of $(B_{12})CBC$ and $(B_{12})CBB$. We also compared the linear and bent C-B-B chain effect in the asymmetric twinned structure. We then examined the deformation and failure mechanisms of these "asymmetric twins" in $B_{vr}BC$ under both pure shear and biaxial shear conditions. The major findings include:

- Under pure shear deformation the asymmetric twinned structures have a lower ideal shear strength than those of single crystals $(B_{12})CBC$ and $(B_{12})CBB$, suggesting that the amorphous shear bands prefer to initiate at these weak planar defects in $B_{vr}BC$. The failure mechanism for asymmetric twinned structures involves the interaction of the C-B-B chains with the icosahedral clusters at the TBs.
- Under biaxial shear conditions, the ideal shear strength of the asymmetric twins is higher than that of single crystal $(B_{12})CBB$, but lower than that of single crystal $(B_{12})CBC$. This arises from the different failure mechanism under indentation loading conditions. Particularly, the icosahedra in $(B_{12})CBB$ and TB region are deconstructed by the interaction between both C-B-B and C-B-C chains and the icosahedra in $(B_{12})CBB$ and TB regions in the $(B_{12})CBC-(B_{12})b CBB$ twin. While the icosahedra in both $(B_{12})CBB$ and $(B_{12})CBC$ regions are deconstructed yet the icosahedra in TB region remains intact in $(B_{12})CBC-(B_{12})l CBB$ asymmetric twin because of the interactions of both C-B-B and C-B-C chains with icosahedra in the layer II regions.

Summarizing our studies on nanotwins in boron carbides, the asymmetric twin in B_4C is actually the phase boundary of ground state structure $(B_{11}C_p)CBC$ and high energy structure of $(B_{11}C_e)CBC$. While the asymmetric twin in $B_{vr}BC$ is the phase boundary of $(B_{12})CBC$ and $(B_{12})CBB$ in which the CBB chain can be linear or kink. Only symmetric twin can be observed in $B_{13}C_2$ because of the relative simple configuration of $(B_{12})CBC$. Nanotwins can strengthen the

B_4C, even exceed the ideal shear strength, but they can impair the strength of $B_{13}C_2$ and $B_{vr}BC$ structures.

Acknowledgements

This work is supported by the National Science Foundation (CMMI−1727428, program manager, Siddiq Qidwai).

References

1 Q. Yu, L. Qi, K. Chen, R. K. Mishra, J. Li and A. M. Minor, The nanostructured origin of deformation twinning, *Nano Lett.*, 2012, **12**, 887–892.

2 K. Lu, L. Lu and S. Suresh, Strengthening materials by engineering coherent internal boundaries at the nanoscale., *Science*, 2009, **324**, 349–352.

3 A. Nie, L. Y. Gan, Y. Cheng, Q. Li, Y. Yuan, F. Mashayek, H. Wang, R. Klie, U. Schwingenschlogl and R. Shahbazian Yassar, Twin Boundary-Assisted Lithium Ion Transport, *Nano Lett.*, 2015, **15**, 610–615.

4 L. Lu, X. Chen, X. Huang and K. Lu, Revealing the maximum strength in nanotwinned copper, *Science*, 2009, **323**, 607–610.

5 K. C. Kim, J. Lee, B. K. Kim, W. Y. Choi, H. J. Chang, S. O. Won, B. Kwon, S. K. Kim, D. Bin Hyun, H. J. Kim, H. C. Koo, J. H. Choi, D. I. Kim, J. S. Kim and S. H. Baek, Free-electron creation at the 60° twin boundary in Bi2Te3, *Nat. Commun.*, 2016, **7**, 12449.

6 Y. Tian, B. Xu, D. Yu, Y. Ma, Y. Wang, Y. Jiang, W. Hu, C. Tang, Y. Gao, K. Luo, Z. Zhao, L. M. Wang, B. Wen, J. He and Z. Liu, Ultrahard nanotwinned cubic boron nitride,

Nature, 2013, **493**, 385–388.

7 B. Li, H. Sun and C. Chen, Large indentation strain-stiffening in nanotwinned cubic boron nitride, *Nat. Commun.*, 2014, **5**, 4965.

8 T. Fujita, P. Guan, K. M. Reddy, A. Hirata, J. Guo and M. Chen, Asymmetric twins in rhombohedral boron carbide, *Appl. Phys. Lett.*, 2014, **104**, 21907.

9 K. Y. Xie, Q. An, M. F. Toksoy, J. W. McCauley, R. A. Haber, W. A. Goddard III and K. J. Hemker, Atomic-Level Understanding of 'asymmetric Twins' in Boron Carbide, *Phys. Rev. Lett.*, 2015, **115**, 175501.

10 M. W. Chen, J. W. McCauley and K. J. Hemker, Shock-Induced Localized Amorphization in Boron Carbide, *Science*, 2003, **299**, 1563–1566.

11 K. M. Reddy, P. Liu, A. Hirata, T. Fujita and M. W. Chen, Atomic structure of amorphous shear bands in boron carbide, *Nat. Commun.*, 2013, **4**, 2483.

12 N. Vast, J. Sjakste and E. Betranhandy, Boron carbides from first principles, *J. Phys. Conf. Ser.*, 2009, **176**, 12002.

13 V. Domnich, S. Reynaud, R. A. Haber and M. Chhowalla, Boron carbide: Structure, properties, and stability under stress, *J. Am. Ceram. Soc.*, 2011, **94**, 3605–3628.

14 F. Thevenot, Boron carbide-A comprehensive review, *J. Eur. Ceram. Soc.*, 1990, **6**, 205–225.

15 D. Simeone, C. Mallet, P. Dubuisson, G. Baldinozzi, C. Gervais and J. Maquet, Study of boron carbide evolution under neutron irradiation by Raman spectroscopy, *J. Nucl. Mater.*, 2000, **277**, 1–10.

16 C. Cheng, K. M. Reddy, A. Hirata, T. Fujita and M. W. Chen, Structure and mechanical properties of boron-rich boron carbides, *J. Eur. Ceram. Soc.*, 2017, **37**, 4514–4523.

17 K. Y. Xie, K. Livi, J. W. McCauley and K. J. Hemker, Precipitation of AlN in a commercial hot-pressed boron carbide, *Scr. Mater.*, 2015, **101**, 95–98.

18 J. E. Saal, S. Shang, Z. kui. Liu, J. E. Saal, S. Shang and Z. Liu, The structural evolution of boron carbide via ab initio calculations The structural evolution of boron carbide via ab initio calculations, *Appl. Phys. Lett.*, 2007, **91**, 231915.

19 M. W. Chen, J. W. McCauley, J. C. LaSalvia and K. J. Hemker, Microstructural characterization of commercial hot-pressed boron carbide ceramics, *J. Am. Ceram. Soc.*, 2005, **88**, 1935–1942.

20 M. Bouchacourt and F. Thevenot, The properties and structure of the boron carbide phase, *J. less common Met.*, 1981, **82**, 227–235.

21 D. Gosset and M. Colin, Boron carbides of various compositions: An improved method for X-rays characterisation, *J. Nucl. Mater.*, 1991, **183**, 161–173.

22 M. Beauvy, Stoichiometric limits of carbon-rich boron carbide phases, *J. Less Common Met.*, 1983, **90**, 169–175.

23 Q. An and W. A. Goddard III, Nanotwins soften boron-rich boron carbide (B13C2), *Appl. Phys. Lett.*, 2017, **110**, 111902.

24 Q. An, W. A. Goddard III, K. Y. Xie, G. D. Sim, K. J. Hemker, T. Munhollon, M. Fatih Toksoy and R. A. Haber, Superstrength through Nanotwinning, *Nano Lett.*, 2016, **16**, 7573–7579.

25 X. Yang, W. A. Goddard III and Q. An, Structure and Properties of Boron-Very-Rich Boron Carbides: B12 Icosahedra Linked through Bent CBB Chains, *J. Phys. Chem. C*, 2018, **122**, 2448–2453.

26 G. Kresse and J. Hafner, Ab initio molecular dynamics for liquid metals, *Phys. Rev. B*, 1993, **47**, 558–561.

27 G. Kresse and J. Furthmüller, Efficient iterative schemes for ab initio total-energy calculations using a plane-wave basis set, *Phys. Rev. B*, 1996, **54**, 11169–11186.

28 G. Kresse and J. Furthmüller, Efficiency of ab-initio total energy calculations for metals and semiconductors using a plane-wave basis set, *Comput. Mater. Sci.*, 1996, **6**, 15–50.

29 G. Kresse, From ultrasoft pseudopotentials to the projector augmented-wave method, *Phys. Rev. B*, 1999, **59**, 1758–1775.

30 D. Roundy, C. Krenn, M. Cohen and J. Morris, Ideal Shear Strengths of fcc Aluminum and Copper, *Phys. Rev. Lett.*, 1999, **82**, 2713–2716.

31 Q. An, W. A. Goddard III and T. Cheng, Atomistic Explanation of Shear-Induced Amorphous Band Formation in Boron Carbide, *Phys. Rev. Lett.*, 2014, **113**, 95501.

32 Q. An and W. A. Goddard III, Atomistic Origin of Brittle Failure of Boron Carbide from Large-Scale Reactive Dynamics Simulations: Suggestions toward Improved Ductility, *Phys. Rev. Lett.*, 2015, **115**, 105501.